J Sol-Gel Sci Technol (2012) 64:694–703
DOI 10.1007/s10971-012-2904-6

ORIGINAL PAPER

Evaluation of in vitro bioactivity and MG63 Oesteoblast cell response for TiO_2 coated magnesium alloys

P. Amaravathy · C. Rose · S. Sathiyanarayanan · N. Rajendran

Received: 10 May 2012 / Accepted: 15 October 2012 / Published online: 9 November 2012

Abstract The present investigation reports TiO_2 coating on magnesium alloy AZ31 by sol–gel method via dip coating technique. TiO_2 coated surface was characterized by thin film X-ray diffraction (TF-XRD), Fourier transform infrared red (FT-IR) spectroscopy, scanning electron microscopy (SEM) with energy-dispersive X-ray (EDX) spectroscopy, atomic force microscopy (AFM) and transmission electron microscopy (TEM) techniques. From TF-XRD results, the peaks at 2θ values of 25.14, 32.12, 68.73 and 70.11 confirm the presence of TiO_2. The TiO_2 is crystalline in nature and the crystallite size is about 32.4 nm. SEM-EDX, TEM and AFM show that the coated surface is uniform and nanoporous. FT-IR analysis shows that the peak in the range of 692 cm^{-1} is assigned to Ti–O–Ti stretching vibration. Contact angle measurements show that the coating is hydrophilic in nature. Bioactivity of the coating in simulated body fluid (SBF) was also examined, the hydroxyl functionalized surface greatly enhances the hydroxyapatite growth. The potentiodynamic polarization studies prove that the corrosion resistance of the TiO_2 coated surface after immersion in SBF for 7 days is improved dramatically. Cell adhesion studies confirm the increased cell attachment on TiO_2 coated surface when compared to uncoated alloy, due to less amount of Mg ion release from the substrate in the culture medium.

Keywords Magnesium alloy · Sol–gel · Hydrophilicity · Biocompatibility · Contact angle · Oesteoblast cells

1 Introduction

In recent years, there has been increasing interest in magnesium alloys, used as a potential biodegradable implant material due to their favorable properties. Magnesium is light in weight [1], nontoxic, biocompatible [2] and its mechanical properties like fracture toughness, elastic modulus, comparative strength [3, 4] are similar to natural bone. Magnesium is also one of the important ions for the formation of biological apatite and involved in bone metabolism [5]. However, higher degradation rate of magnesium alloy due to corrosion in the complex physiological environment limits its application [6]. The high dissolution rate of magnesium leads to undesirable development of hydrogen gases and subsequent pH increase is the complicated phenomenon to be dealt with by the host tissue. For the safe usage of magnesium as a biodegradable implant, its corrosion rate should be controlled and this can be achieved by means of surface modification techniques. Thermal spraying [7], ion implantation [8], electrodeposition [9], plasma surface modification [10], laser irradiation [11], physical vapour deposition [12] and chemical vapour deposition [13] are some of the surface modification techniques available to deposit the thin film on magnesium alloy. These techniques have several disadvantages such as high cost-to-benefit ratio, high temperature or environmental adverse effects. However, sol–gel is a versatile technique to provide effective coatings with improved

P. Amaravathy · N. Rajendran (✉)
Department of Chemistry, Anna University, Chennai 600 025, India
e-mail: nrajendran@annauniv.edu

C. Rose
CSIR-Central Leather Research Institute, Adyar, Chennai 600 020, India

S. Sathiyanarayanan
Corrosion Testing and Evaluation Division, CSIR-Central Electrochemical Research Institute, Karaikudi 630 006, India

properties [14]. The main advantages of sol–gel techniques are cost effective, good adherence and homogeneity. ZrO_2 [15], Al_2O_3/Al [16], ZrO_2-CeO_2 [17], Al/SiC [18] protective coatings have been made on magnesium alloys by various processes. Nano TiO_2 was coated on magnesium alloy AZ31 by sol–gel method and made an attempt to relate the corrosion of coated alloys with annealing treatment and resultant structural evolution was reported [19]. So far, there are no research findings on in vitro corrosion evaluation and cell adherence on sol gel nano TiO_2 coated magnesium alloy AZ31. Earlier reports show that TiO_2 is bioactive, inducing fast deposition of apatite from SBF solution [20]. Hence, in the present work, TiO_2 was coated on magnesium alloy AZ31 using sol–gel method and its in vitro corrosion evaluation, bioactivity and cell attachment capacity was studied.

2 Materials and methods

2.1 Substrate pretreatments

The substrate material used for the present study is AZ31 magnesium alloy and its chemical composition is shown in Table 1. The samples with the dimensions of 22 mm × 15 mm × 2 mm were polished to a 1,200 grit of SiC paper and thoroughly washed with distilled water and ultrasonically degreased with acetone followed by methanol for 5 min to remove any organic matter and dust particle present on the surface and dried with hot air.

2.2 TiO_2 preparation and coating formation

The nano TiO_2 was prepared by sol–gel method. Reagent grade chemicals were purchased from Alfa aesar and were used in the preparation procedure without further purification. The starting compounds were tetra isopropyl ortho titanate, isopropyl alcohol, acetylacetone, nitric acid and double distilled water and the molar ratio of the compounds was 1:10:0.7:0.3:0.01 respectively. Tetra iso propyl ortho titanate was dissolved in pure isopropyl alcohol in a round bottom flask and stirred at 60 °C for 2 h. To the above contents, acetylacetone was added drop wise as a chelating agent to control the hydrolysis rate of tetra isopropyl ortho titanate. The contents were continuously stirred for 6 h. A small amount of HNO_3 was introduced as a catalyst to increase the reaction rate and distilled water was added during stirring to complete the hydrolysis. After cooling down to room temperature, the obtained sol was used for dip coating of the magnesium alloy substrates. The sol–gel TiO_2 thus obtained on AZ31 substrate was later dried in an oven at 60 °C for 1 h for the gelation process. Then, the substrates were sintered at 120, 240, and 360 °C for 1 h. The procedure used for the preparation of TiO_2 was similar to those reported [21].

Table 1 Chemical composition of magnesium alloy AZ31

Elements	Al	Zn	Mn	Cu	Mg
Wt%	2.83	0.8	0.37	0.002	Balance

2.3 Surface characterization

The TiO_2 coating and the hydroxyapatite grown on the substrate after 7 days have been carefully scrapped off from the substrate and were carried out in the range of 400–4,000 cm^{-1} on FTIR (Thermo Electron Corporation, USA) using KBr pellet technique. Thin film X-ray diffraction analysis was carried out on a PAN Analytical X-Pert Pro Diffractometer using Cu Kα (2.2 KW max) at a scan rate of 0.02°. Scanning Electron Microscopy with Energy-dispersive X-ray spectroscopy (Hitachi Model-S3400) was used to characterize the surface morphology and elemental composition of TiO_2 coating. Atomic Force Microscopy measurements were carried out using SII (Seiko instruments, Japan) by non-contact mode using Au coated Si cantilevers with the spin constant of 1.6 N/m as a resonance frequency of 26 kHz under air atmosphere at room temperature. The transmission electron microscopy (TEM) images were obtained with a JEOL1200EX high resolution transmission electron microscope using tungsten electron source and built-in camera with electron image film. The hydrophilicity of TiO_2 coatings in SBF were measured by Euroma optical microscope with inbuilt colour charge coupled device (CCD) camera and wetting profile of the photograph of the sessile drop was analyzed in the digital image with the help of 'image J' software and the standard deviation due to experimental error was calculated as ±3°. Hydrogen evolution test was carried out to study the degradation rate and volume of hydrogen evolved from coated and uncoated AZ31. The procedure for conducting the experiments was according to the earlier report [22].

2.4 Electrochemical characterization

The conventional three electrode cell was used for all the corrosion evaluation measurements. A saturated calomel electrode (SCE) was used as a reference electrode, platinum foil as a counter electrode and the test material as a working electrode. The preparation of SBF and the procedure for electrochemical experiment and the in vitro studies were carried out according to the earlier report [23]. SBF was used as an electrolyte for the potentiodynamic polarisation studies. Potentiostat (Model PGSTAT 12, The

Netherlands B.V) was controlled by a personal computer with software GPES Version 6.0 used for conducting the experiments and the polarization curves were scanned from −2,000 mV/SCE to −200 mV at a scan rate of 1 mV/s. In order to test the reproducibility, tests were performed in triplicate.

2.5 Cell adhesion test

All the substrates used in this study were autoclaved to avoid contamination. To test the cell adhesion behaviour on coated alloy for 7 days, polished and chemically cleaned AZ31 were used as a control group. MG63 oesteoblast-like cells were procured from National Centre for Cell Science (NCCS) Pune and cultured with Dulbecco's Modified Eagle Medium (DMEM, Gibco, USA) with supplements of 10 % fetal bovine serum (FBS), 100 µg/ml unit of penicillin and streptomycin under standard cell culture conditions until they reached confluent state. When the proliferation reached sufficient quantity, they were used for the experiments. 1.7×10^4 cells were seeded on each well and cultured at 37 °C with 5 % CO_2 for 7 days. Experiment was done as a triplicate. The medium was removed and 100 µl of working solution was added followed by the addition of ethidium bromide/acridine orange (a mixture of acridine orange and ethidium bromide 1:1, 1 mg/ml). After 5 min, the cell attachment was assessed under fluorescence microscope (Leica DM IRB-Camera Leica DFC) that captures the wavelength emission at 540 nm and excitation at 600 nm. The number of cells attached to each sample was quantified using an image analysis system (OMNIMET).

3 Results and discussion

3.1 FTIR analysis

FTIR spectra of TiO_2 coated magnesium alloy sintered at various temperatures are shown in Fig. 1. Maximum height of the peak was observed at 360 °C and hence, the sintering temperature of the substrate maintained was 360 °C throughout the experiments. Broad peak between 3,500 and 3,300 cm^{-1} is assigned to fundamental stretching vibration of O–H groups. The peak at 1,450 cm^{-1} is related to C–H deformation and the bending vibrations of H–O–H bond are formed at 1,614 cm^{-1}, which is due to chemisorbed water. The TiO_2 coating shows a strong peak at 692 cm^{-1}, which is due to Ti–O and Ti–O–Ti groups that confirm the formation of TiO_2 on the substrate [24]. FTIR spectrum of TiO_2 coating after immersion in SBF is shown in Fig. 2. The absorption peak at 563 cm^{-1} with a small shoulder at 476 cm^{-1} are associated to the deformation vibration of

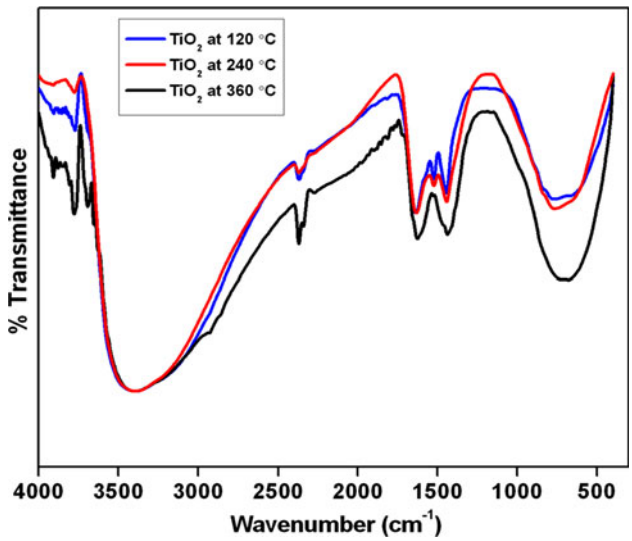

Fig. 1 FTIR Spectra of TiO_2 coated AZ31 substrate sintered at (a) 120 °C (b) 240 °C and (c) 360 °C for 1 h

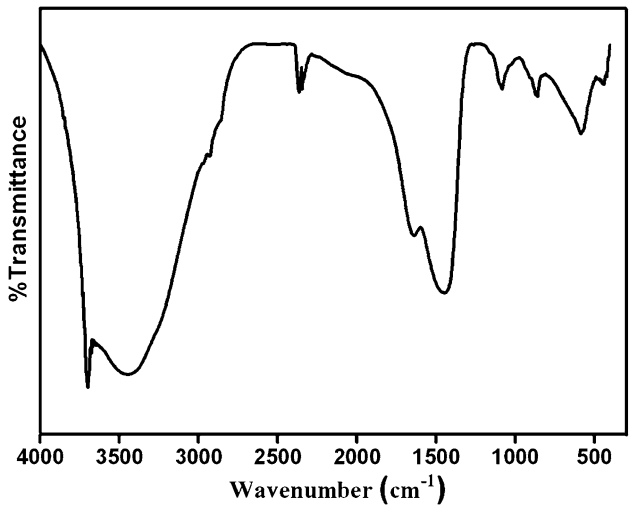

Fig. 2 FTIR Spectra of TiO_2 coated AZ31 substrate after immersion in SBF for 7 days

P–O in the PO_4 group indicating an apatite structure. The band at 1,120 cm^{-1} is assigned to P–O stretching modes. There is a small absorption band at 840 cm^{-1}, which belongs to HPO_4^{2-} group. The strong band at 1,452 cm^{-1} with a shoulder at 1,654 cm^{-1} are due to CO_3^{2-} group of hydroxyapatite [25]. These peaks confirm the deposition of hydroxyapatite from SBF solution.

3.2 Thin film X-ray diffraction studies

The TF-XRD pattern of TiO_2 coated magnesium alloy is shown in Fig. 3. The peaks at 2θ values of 25.14, 32.12, 68.73 and 70.11 with the orientation along (101), (110),

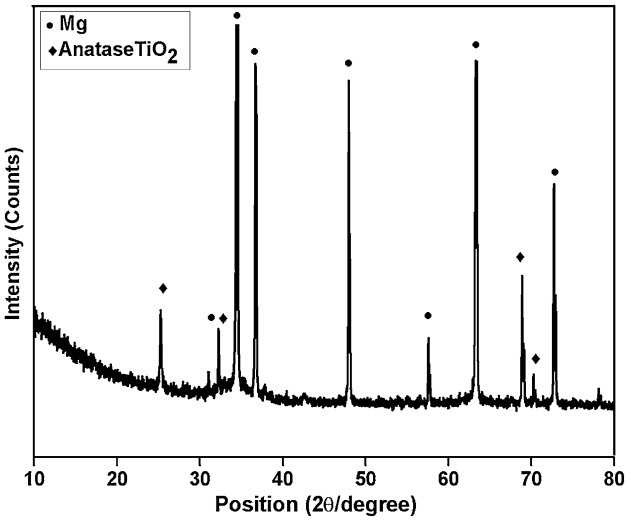

Fig. 3 TF-XRD pattern of AZ31 substrate with TiO_2 coating

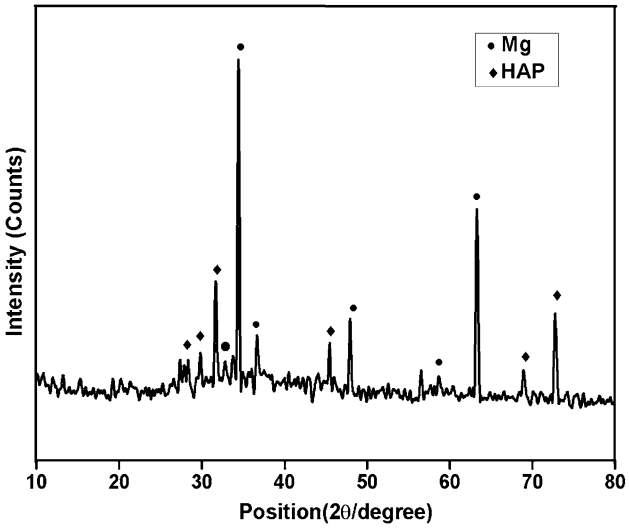

Fig. 4 TF-XRD pattern of hydroxyapatite deposited over AZ31 after immersion in SBF for 7 days

(116) and (220) planes represent anatase phase of TiO_2. The obtained results are in good agreement with the JCPDS data (JCPDS Card No 89-4203). The peak at (101), which was the most distinct reflection was chosen to calculate the crystallite size using Scherrer's equation $d_{hkl} = k\lambda/B\ \cos 2\theta$ [26]. The calculated crystallite size is in the range of 32.4 nm and the peaks indicate that they are crystalline in nature. Because of the porous nature of the coating, the dominating peaks are also originating from magnesium alloy surface. The XRD pattern of TiO_2 after immersion in SBF is shown in Fig. 4. Besides the peak of magnesium and TiO_2 coating, new peaks appeared at 2θ value of 28.29, 31.68, 32.81, 45.44, 68.84 and 72.88 corresponding to preferential planes of HA (JCPDS-89-6440). The results show the formation of hydroxyapatite from SBF solution.

3.3 Atomic force microscopy

Figure 5 represents that TiO_2 coating changed the surface topography significantly. The coating is porous and consists of nanometer sized particles. The particle size could be in the range of 30 nm. Pores are formed due to difference in thermal expansion coefficient during heat treatment [27]. However, porosity has great influence on the bioactivity of the coating and RMS roughness value of the coating is 0.1334 nm, which is higher than the bare substrate (0.1053 nm). For the sake of brevity, the image of bare substrate is not given. Changes in the roughness value prove that there is a significant modification has occurred in the topography and roughness has shown to be one of the important features for cell growth. Invitro studies also proved that rough porous surface favours the osseointegration [28] and hence, TiO_2 coated AZ31 surface is more bioactive than the uncoated surface.

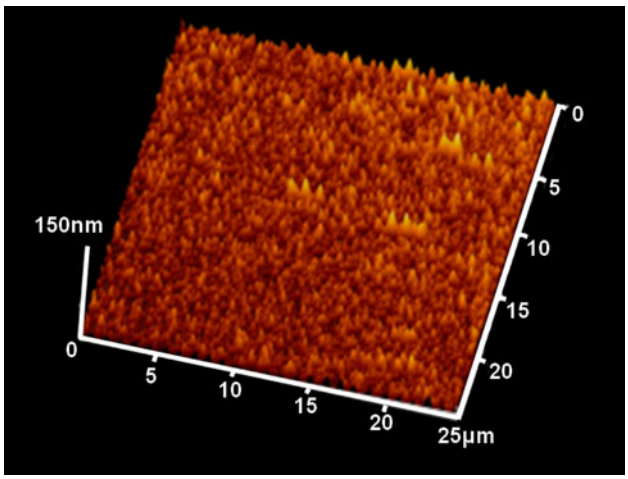

Fig. 5 AFM micrograph of TiO_2 coated AZ31

3.4 Scanning electron microscopy

Figure 6a shows the uncoated magnesium alloy surface with small streaks due to mechanical polishing. Corresponding EDX analysis shows the elemental composition of the substrate surface. Figure 6b shows that TiO_2 coated surface is multilayered with uniformly distributed pores and cracks, which are formed during sintering process. Due to porous nature of the coating, EDX also shows the presence of magnesium peak with corresponding Ti element [29]. However, the intensity of magnesium peak is greatly decreased in contrast to uncoated substrate. The uncoated and coated substrates were immersed in SBF for 7 days and the surface was examined. Figure 7a shows that the uncoated surface exhibits a cracked morphology on the surface during immersion period due to severe attack of

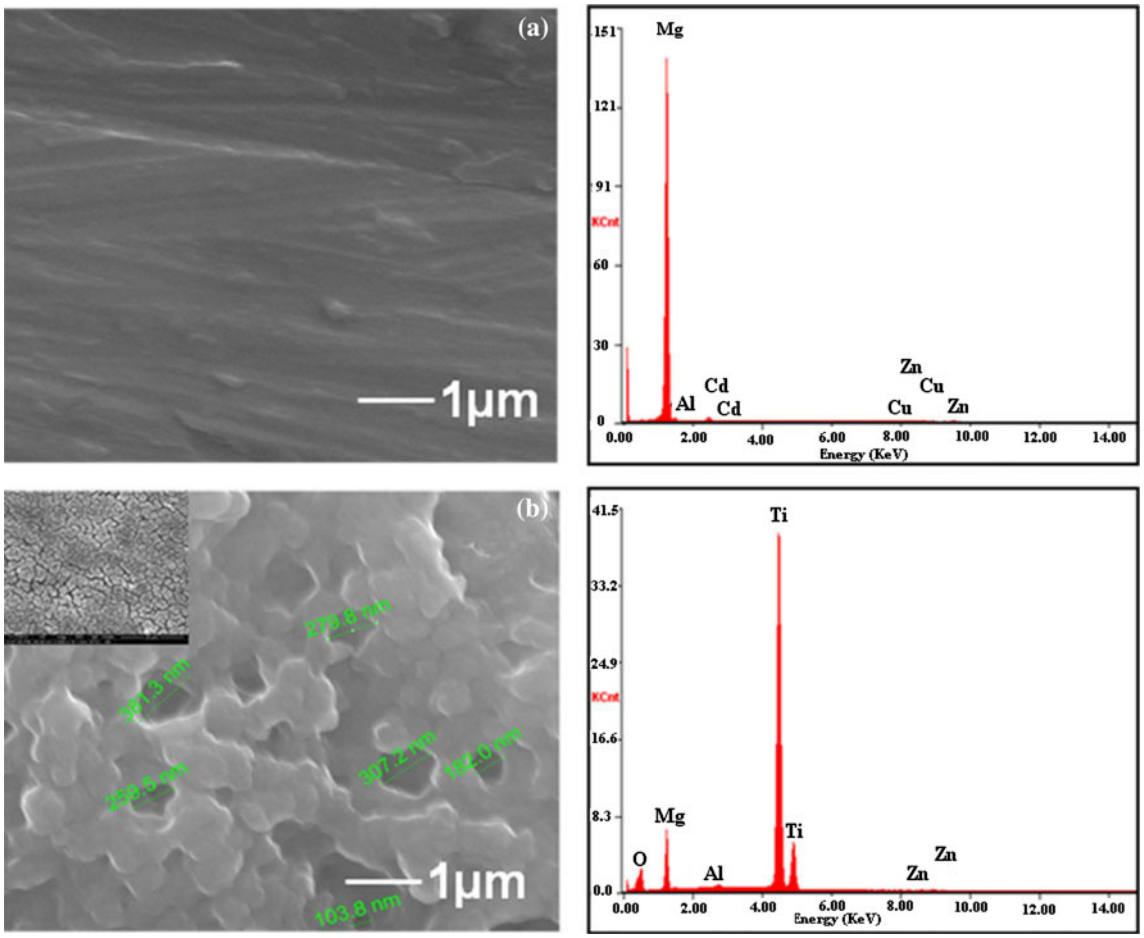

Fig. 6 SEM-EDX analysis of **a** uncoated AZ31, **b** TiO_2 coated AZ31

corrosion. There is no white globule like particles appeared on the substrate. Figure 7b–e shows the coated alloy during immersion in SBF for 7 days. In contrast to uncoated substrate, the coated surface shows less corrosion attack with milder cracks of the coating. However, severe cracks with wider gaps appeared at fifth day, the coating integrity is maintained. It can be noticed that severe collapses in the coating occurs and white particles are found at the isolated places at seventh day. It is obvious that the deposited particles are apatite particles, which are confirmed from EDX results and which are well coincided with the XRD results. Figure 7f shows the apatite deposits which are an important mineral component of bone and which enhance ossification process. The formation of apatite on TiO_2 coated surface is a well familiar mechanism that the Ti–OH groups formed on the surface during immersion promote the formation of apatite by subsequent absorption of Ca^{2+} and PO_4^{3-} ions [30]. It is found that the Ca/P ratio is less than the biological apatite due to magnesium substitution. Such type of magnesium substituted hydroxyapatite has a significant impact on the HA crystal formation and diminishes the magnesium deficiency and which in turn eliminates the osteoporosis in humans [31].

3.5 Transmission electron microscopy

Transmission electron microscopy and SAED pattern of TiO_2 coated alloy calcined at 360 °C are shown in Fig. 8. It can be seen that the TiO_2 nano particles are irregular in shape and agglomerated into clusters. The particle size cannot be estimated due to the aggregation. From SAED pattern, it can be confirmed that it is crystalline in nature and the fringes of (101) and (200) planes are well coincided with the planes obtained in XRD results.

3.6 Contact angle measurements

The contact angle measurements of uncoated and TiO_2 coated surface are shown in Fig. 9. The contact angle value of uncoated alloy is found to be 68° whereas, the contact angle of coated alloy is 23°. Low value of the contact angle suggests the

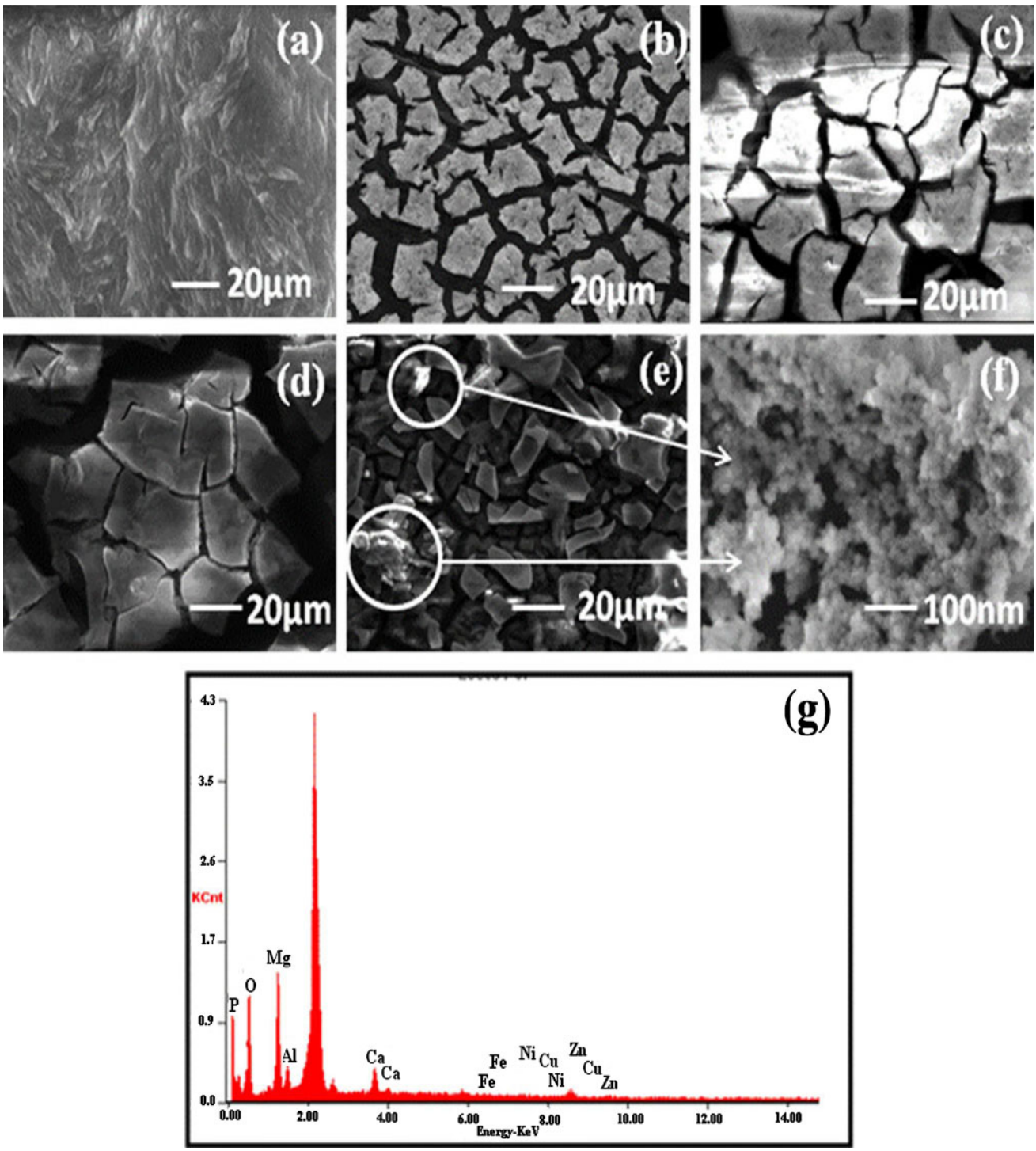

Fig. 7 SEM morphology of **a** Uncoated AZ31 **b** TiO_2 coated AZ31 after immersion in SBF for 1st day **c** 3rd day **d** 5th day **e** 7th day **f** Magnified image of the *circled* part of **e** shows the hydroxyapatite growth **g** EDX analysis of Hydroxyapatite growth

higher surface energy of the TiO_2 films synthesized by sol–gel technique [32–34]. Hence, when a drop of SBF is placed, it evenly spreads over the surface exhibiting highly hydrophilic nature and induces effective apatite growth.

3.7 Hydrogen evolution studies and pH measurements

Hydrogen evolution and pH increase was studied to estimate the degradation rate of magnesium alloy AZ31.

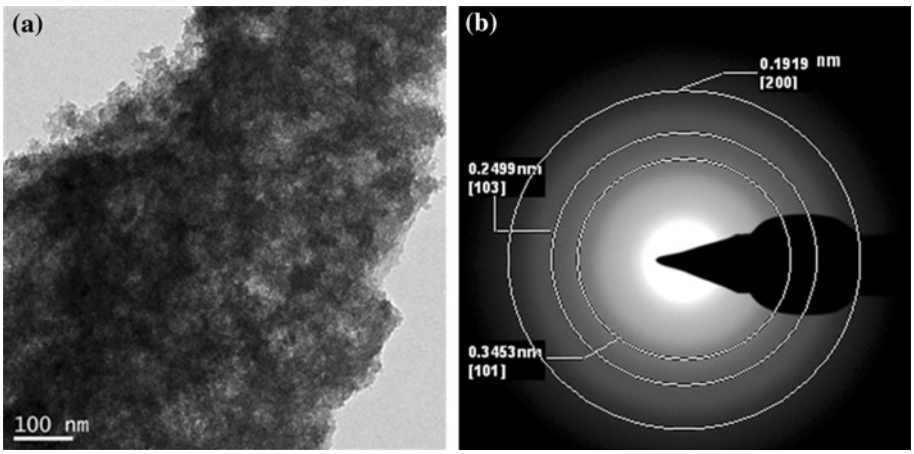

Fig. 8 **a** TEM image and **b** SAED pattern of TiO_2 coated AZ31

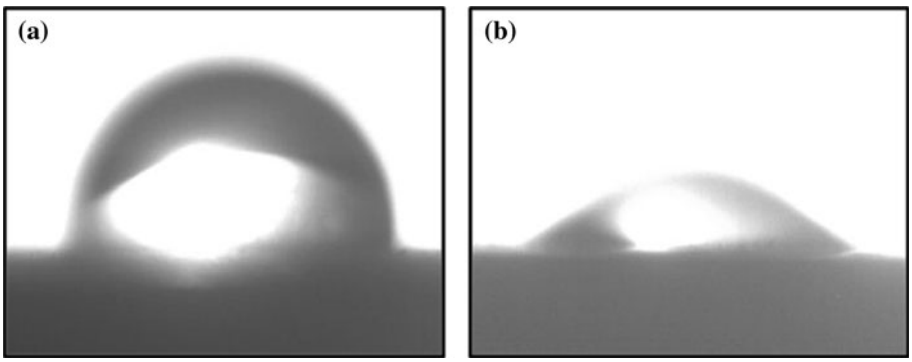

Fig. 9 Contact angle measurement of **a** uncoated **b** TiO_2 coated exhibiting hydrophobic and hydrophilic nature, respectively

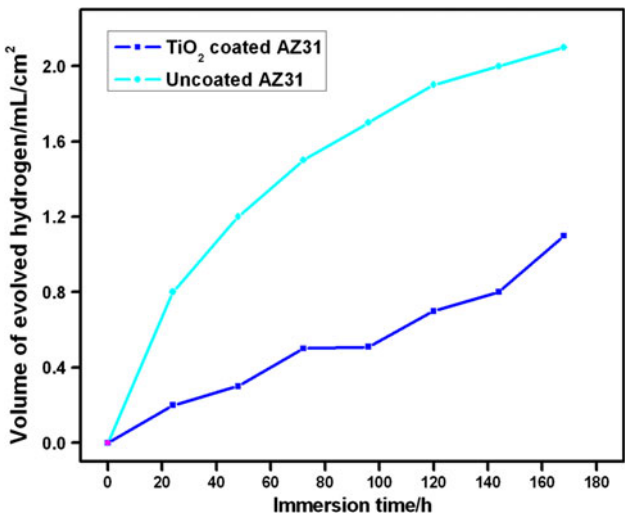

Fig. 10 Degradation rate of uncoated and TiO_2 coated AZ31 immersed in SBF for 7 days

Hydrogen evolution test is trustworthy and not prone to errors in contrast to weight loss method. In addition, rate of degradation with time can be calculated. Figure 10 shows the hydrogen evolution tendency of uncoated and coated alloy during immersion in SBF for 7 days and the initial pH of the SBF maintained was 7.4.

Table 2 pH increase of the uncoated and TiO_2 coated alloy immersed in SBF for 7 days

Days:	1	2	3	4	5	6	7
Uncoated	7.6	7.9	8.1	8.3	8.4	8.6	8.9
Coated	7.6	7.6	7.7	7.8	7.8	7.9	8.0

It can be seen that uncoated magnesium alloy exhibits faster degradation rate than the TiO_2 coated alloy. In case of uncoated magnesium alloy, bubbles are coming from the substrate surface after few minutes and the substrate started to damage. As time progresses, corrosion products are clearly visible and continuous film was formed with small pits. The corrosion products may be released Mg^{2+} ions, alkalization of solution by OH^- ions and released alloying metal elements. At the seventh day, the substrate is severely damaged and totally covered with corrosion product and the total volume of hydrogen collected is 2.1 ml. In case of TiO_2 coated magnesium alloy AZ31, very few bubbles are observed up to 2 days and after prolonged immersion of 2 days, even though the corrosion rate is increased, no corrosion product is visible. At seventh day, local collapses of TiO_2 coating occur and exhibited

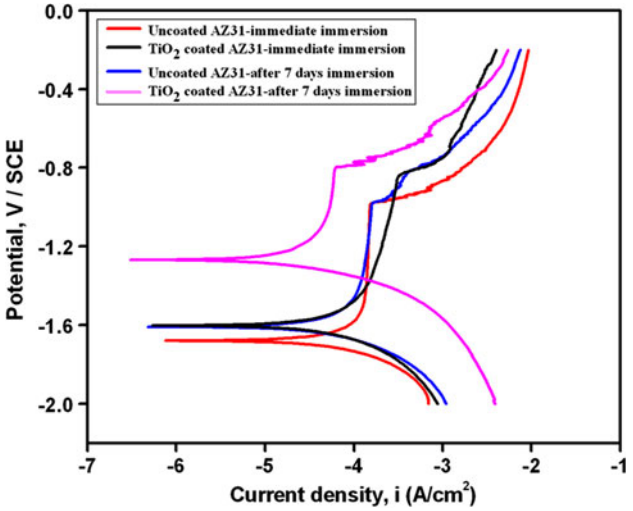

Fig. 11 Potentiodynamic plots of AZ31 and TiO_2 coated AZ31before and after immersion in SBF for 7 days

tolerable rate of corrosion compared to uncoated alloy. The total volume of hydrogen collected over the period of 7 days is 1.1 ml.

Silver et al. [35] studied the effects of pH on oesteoblast proliferation and differentiation into bone cells. Previous studies indicated that osseointegration is modulated by pH of the physiological medium. Table 2 shows pH of SBF containing TiO_2 coated and uncoated AZ31 and pH increase also shows similar trend as hydrogen evolution rate. Hence the lower hydrogen release rate and pH increase confirms that the degradation rate of TiO_2 coated AZ31 is greatly reduced and it can act as a favorable medium for cellular activity.

Table 3 The electrochemical parameters of potentiodynamic polarization curves of uncoated alloy, TiO_2 coated alloy before and after immersion in SBF for 7 days

	E_{corr}	I_{corr}
Uncoated AZ31	1.729	7.019×10^{-5}
TiO_2 coated AZ31	−1.608	5.267×10^{-5}
Uncoated AZ31 in SBF	−1.602	4.917×10^{-5}
TiO_2 coated in SBF	−1.269	1.874×10^{-5}

3.8 Potentiodynamic polarization studies

Potentiodynamic polarization curves obtained from uncoated and coated AZ31 substrates before and after immersion in SBF are displayed in Fig. 11. It could be seen that the corrosion potential (E_{corr}) of uncoated substrate is more negative of −1.729 mV, while the TiO_2 coated alloy shows a nobler shift to the E_{corr} value of −1.608 mV. The positive potential shift and decrease in current density shows that the corrosion resistance of TiO_2 coated alloy improved significantly. The electrochemical parameters of potentiodynamic polarization

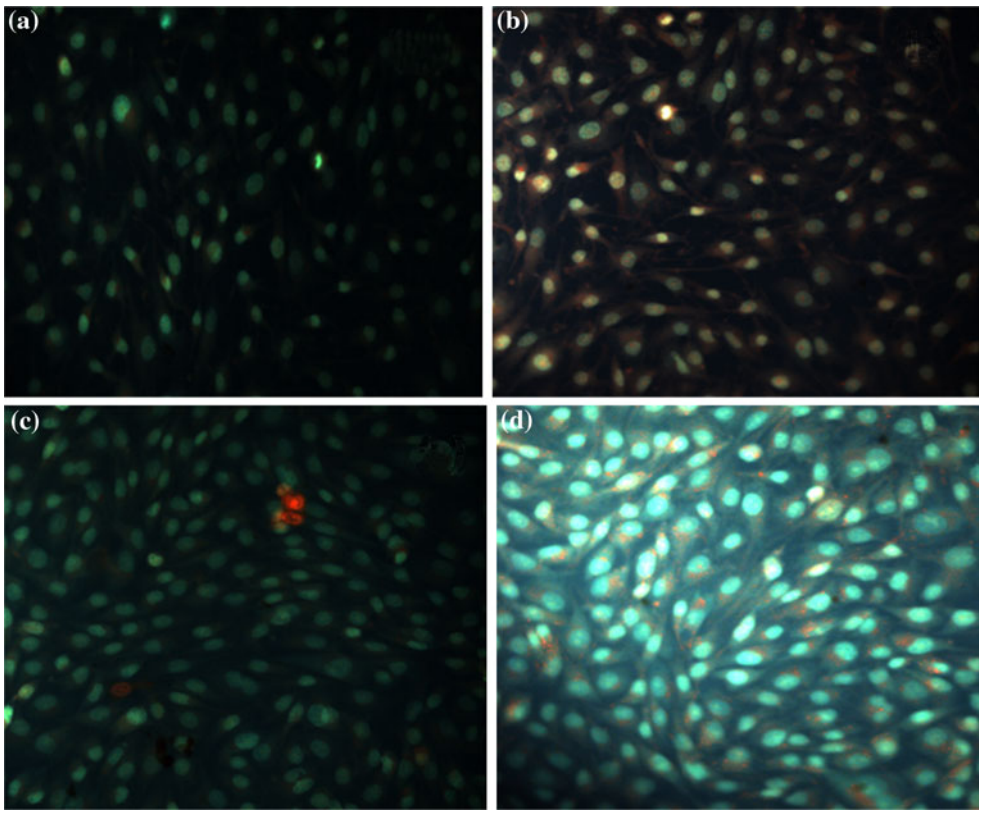

Fig. 12 Fluorescence images of MG-63 oesteoblast like cells growing on each substrate after culturing for 7 days. **a** Uncoated AZ31-1st day **b** TiO_2 coated AZ31-1st day **c** Uncoated AZ31-7th day **d** TiO_2 coated AZ31-7th day

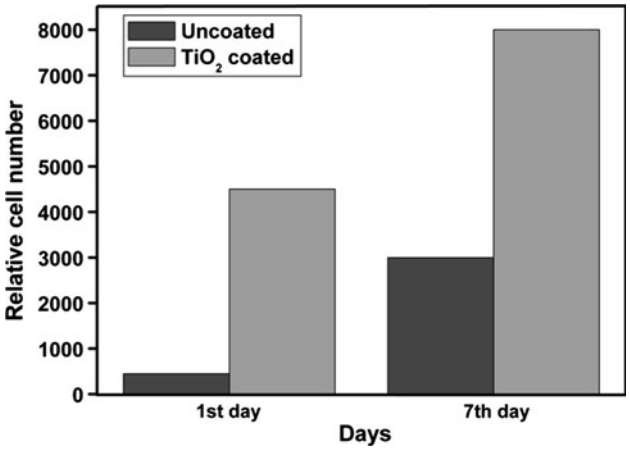

Fig. 13 Relative number of cells attatched on the uncoated AZ31 and coated AZ31 alloys for 7 days

curves are given in Table 3. After 7 days immersion in SBF, TiO_2 coated surface shows the E_{corr} value of −1.602 mV and uncoated shows the E_{corr} value of −1.269 mV. Corrosion potential shifted towards nobler direction and E_{corr} shift was about 0.333 mV. It can be concluded that the HA deposited on the TiO_2 coating could control the diffusion of electrolyte into the substrate and thereby decrease the degradation rate and enhance the potential of TiO_2 coated alloy dramatically when compared to uncoated alloy.

3.9 Cell culture test

Cell culture test is an essential requirement for any material to act as an implant to perform its biological function appropriately. The interactive surface characters such as roughness and chemical composition plays an important role for cell attachment and differentiation. The cell adhered on coated and uncoated AZ31 are shown in Fig. 12. From the fluorescence images, it can be visualized that the cells were more spread and occupy a larger area in the coated alloy when compared to uncoated alloy. The quantitative results of cell attachment test are shown in Fig. 13. It can be clearly seen that number of cells adhered to coated surface is significantly higher than the uncoated surface for first as well as seventh day, which is due to the alteration in the surface topography, contributing to higher degree of interaction with bone cells. The presence of Ti–OH group of the coating has a higher potential in attracting the osteoblast cells in presence of DMEM medium and induces the bone growth rapidly [36–38].

4 Conclusions

TiO_2 coating was successfully deposited on AZ31 by sol–gel dip coating technique. XRD pattern proves that the anatase TiO_2 is crystalline in nature. Surface characterization studies show that the coating is multilayered and consists of nanometer sized particles. Lower contact angle of TiO_2 coating reveals its superior wettability and improved biocompatibility. The immersion studies shows that the Ti–OH group formed on TiO_2 showed the ability to induce the apatite formation in SBF. Potentiodynamic polarization and Hydrogen evolution studies show the better corrosion resistance and lower degradation rate of TiO_2 coated AZ31. Cell culture studies depict that better cell adhesion was observed on coated specimen by more cell spreading and greater degree of cell attachment. Hence, the TiO_2 coated AZ31 can be a useful route as an artificial bone substitute due to their enhanced bioactivity and better adhesion to bone cells.

Acknowledgments One of the authors, P. Amaravathy would like to acknowledge the Anna University for providing Anna Centenary Research Fellowship to carry out the research work. Department of Science and Technology-Fund for improvement of S & T infrastructure in higher education institutions and University Grant Commission-Departmental Research Support is also greatly acknowledged for instrument facility.

References

1. Zhanga S, Li Q, Chen B, Yang X (2010) Preparation and corrosion resistance studies of nanometric sol–gel-based CeO_2 film with a chromium-free pretreatment on AZ91D magnesium alloy. Electrochim Acta 55:870–877
2. Gray JE, Luan B (2002) Protective coatings on magnesium and its alloys—a critical review. J Alloy Compd 336:88–113
3. Wang J, Wang L, Guan S, Zhu S, Ren C, Hou S (2010) Microstructure and corrosion properties of as sub-rapid solidification Mg-Zn-Y-Nd alloy in dynamic simulated body fluid for vascular stent application. J Mater Sci Mater Med 21:2001–2008
4. Zhang Y, Zhang G, Wei M (2009) Controlling the biodegradation rate of magnesium using biomimetic apatite coating. J Biomed Mater Res B Appl Biomater 89:408–414
5. GU XN, Zheng YF (2010) A review on magnesium alloys as biodegradable materials. Front Mater Sci China 4:111–115
6. Xu L, Zhang E, Yin D, Zeng S, Yang K (2008) In vitro corrosion behaviour of Mg alloys in a phosphate buffered solution for bone implant application. J Mater Sci Mater Med 19:1017–1025
7. Pardo A, Casajús P, Mohedano M, Coy AE, Viejo F, Torres B, Matykina E (2009) Corrosion protection of Mg/Al alloys by thermal sprayed aluminium coatings. Appl Surf Sci 255:6968–6977
8. Zhou H, Chen F, Yang YG, Wan HC, Cai S (2008) Study on process of Ion implantation on AZ31 magnesium alloy. Key Eng Mater 373–374:342–345
9. Chang JK, Chen SY, Tsai WT, Deng MJ, Sun IW (2007) Electrodeposition of aluminum on magnesium alloy in aluminum chloride ($AlCl_3$)-1-ethyl-3-methylimidazolium chloride (EMIC) ionic liquid and its corrosion behavior. Electrochem Commun 9:1602–1606
10. Guan SK, Peng L, Wen CL, Luo Q (2008) Electrochemical fabrication and biocompatibility of the hydroxyapatite coating on magnesium alloy for implanted applications. In: Magnesium technology 2008. pp 367–371
11. Izumi S, Yamasaki M, Otsu M, Kawamura Y (2007) Use of laser irradiation to form anti-corrosive surface oxide layer on Mg. Metal Mater Trans 48:1965–1968

12. Hoche H, Schmidt J, Grob S, Trobmann T, Berger C (2011) PVD coating and substrate pretreatment concepts for corrosion and wear protection of magnesium alloys. Surf Coat Technol 205:S145–S150
13. Christoglou C, Voudouris N, Angelopoulos GN, Pant M, Dahl W (2004) Deposition of aluminium on magnesium by a CVD process. Surf Coat Technol 184:149–155
14. Leite Edson Roberto (2009) Nanostructured materials for electrochemical energy production and storage. Springer Science, New York, USA
15. Li Q, Zhong X, Hu J (2008) Preparation and corrosion resistance studies of zirconia coating on fluorinated AZ91D magnesium alloy. Prog Org Coat 63:222–227
16. Xin Y, Hua K, Hu T, Tans G, Chu PK (2009) Mechanical properties of Al_2O_3/Al bi-layer coated AZ91 magnesium alloy. Thin Solid Films 517:5357–5360
17. Phani AR, Gammel FJ, Hack T, Haefke H (2005) Enhanced corrosion resistance by sol–gel-based ZrO_2-CeO_2 coatings on magnesium alloys. Mater Corros 56:77–82
18. Rodrigo P, Campo M, Torres B, Escalera MD, Otero E, Rams J (2009) Microstructure and wear resistance of Al-SiC composites coatings on ZE41 magnesium alloy. Appl Surf Sci 255:9174–9181
19. Hu J, Zhang C, Cui B, Bai K, Guan S, Wang L, Zhu S (2011) In vitro degradation of AZ31 magnesium alloy coated with nano TiO_2 film by sol–gel method. Appl Surf Sci 257:8772–8777
20. Sun T, Wang M (2008) Low-temperature biomimetic formation of apatite/TiO_2 composite coatings on Ti and NiTi shape memory alloy and their characterization. Appl Surf Sci 255:396–400
21. Milella E, Cosentino F, Liciulli A, Massaro C (2001) Preparation and characterization of titania/hydroxyapatite composite coatings obtained by sol gel process. Biomaterials 22:1425–1431
22. Huo H, Li Y, Wang F (2004) Corrosion of AZ91D magnesium alloy with a chemical conversion coating and electroless nickel layer. Corros Sci 46:1467–1477
23. Kokubo T, Kushitani H, Sakka S, Kitsugi T, Yamamuro T (1990) Solutions able to reproduce in vivo surface-structure changes in bioactive glass-ceramic A-W. J Biomed Mater Res 24:721–734
24. Devi KB, Singh K, Rajendran N (2011) Synthesis and characterization of nanoporous sodium-substituted hydrophilic titania ceramics coated on 316L SS for biomedical applications. J Coat Technol Res 8:595–604
25. Geetha V, Buvaneswari G (2009) Preparation of nanohydroxyapatite by a sol–gel method using alginic acid as a complexing agent. J Am Ceram Soc 92:2207–2211
26. Lindgren T, Muobora JH, Avendeno E, Johnson J, Hoel A, Granquist CG, Lindquist SE (2003) Photoelectrochemical and optical properties of nitrogen doped titanium dioxide films prepared by reactive DC magnetron sputtering. J Phys Chem B 107:5709–5716
27. Sultana R, Yang J, Hu X (2012) Deposition of micro-porous hydroxyapatite/tri-calcium phosphate coating on zirconia-based substrate. J Am Ceram Soc 95:1212–1215
28. Rajeswari R, Ng CCH, Liao S, Pliszka D, Raghunath M, Ramakrishna S, Chan Casey K (2012) Biomimetic surface modification of titanium surfaces for early cell capture by advanced electrospinning. Biomed Mater 7:015001
29. Nagarajan S, Raman V, Rajendran N (2010) Synthesis and electrochemical characterization of porous niobium oxide coated 316L SS for orthopedic applications. Mater Chem Phys 119:363–366
30. Liang F, Zhou L, Wang K (2003) Enhancement of the bioactivity of alkali-heat treated titanium by pre-calcification. J Mater Sci Lett 22:1665–1667
31. Gomes S, Renaudin G, Jallot E, Nedelec J-M (2009) Structural characterization and biological fluid interaction of sol#gel-derived Mg-substituted biphasic calcium phosphate ceramics. Appl Mater Interfaces 2:505–513
32. Bose S, Roy M, Das K, Bandyopadhyay A (2009) Surface modification of titanium for load-bearing applications. J Mater Sci Mater Med 20:S19–S24
33. Kawakami H, Ilala R, Straka L, Papula S, Romu J, Hanninen H, Mahlberg R, Heikkila M (2008) Photocatalytic activity of atomic layer deposited TiO_2 coatings on austenitic stainless steels and copper alloys. J Electrochem Soc 155:C62–C68
34. Sebbowa T, Edirisinghe M, Salih V, Huang J (2011) Effect of deposition parameters and post-deposition annealing on the morphology and cellular response of electrosprayed TiO_2 films. Biofabrication 3:045001
35. Silver IA, Deas J, Erecin′ska M (2001) Interactions of bioactive glasses with osteoblasts in vitro: effects of 45S5 bioglass, and 58S and 77S bioactive glasses on metabolism, intracellular ion concentrations and cell viability. Biomaterials 22:175–185
36. Kim HW, Koh YH, Li LH, Lee S, Kim HE (2004) Hydroxyapatite coating on titanium substrate with titania buffer layer processed by sol-gel method. Biomaterials 25:2533–2538
37. Karpagavalli R, Zhou A, Chellamuthu P, Nguyen K (2007) Corrosion behavior and biocompatibility of nanostructured TiO_2 film on Ti6Al4 V. J Biomed Mater Res A 83:1087–1095
38. Ou J, Wang J, Zhang D, Zhang P, Liu S, Yan P, Liu B, Yang S (2010) Fabrication and biocompatibility investigation of TiO_2 films on the polymer substrates obtained via a novel and versatile route. Colloids Surf B Biointerfaces 76:123–127